RESEARCH ARTICLE

Multimerization of TREM2 is impaired by Alzheimer's disease–associated variants

Hunter B. Dean[1,2,3] | Rory A. Greer[1] | Shan-Zhong Yang[1] | Daniel S. Elston[2] |
Thomas J. Brett[4] | Erik D. Roberson[2] | Yuhua Song[1]

[1]Department of Biomedical Engineering, School of Engineering, University of Alabama at Birmingham, Birmingham, Alabama, USA

[2]Alzheimer's Disease Center, Center for Neurodegeneration and Experimental Therapeutics, & Departments of Neurology and Neurobiology, Marnix E. Heersink School of Medicine, University of Alabama at Birmingham, Birmingham, Alabama, USA

[3]Medical Scientist Training Program, Marnix E. Heersink School of Medicine, University of Alabama at Birmingham, Birmingham, Alabama, USA

[4]Division of Pulmonary and Critical Care Medicine, Department of Internal Medicine, Department of Biochemistry and Molecular Biophysics, Hope Center for Neurological Disorders, & Department of Cell Biology and Physiology, Washington University School of Medicine, Washington University in St Louis, St. Louis, Missouri, USA

Correspondence
Yuhua Song, Department of Biomedical Engineering, School of Engineering, University of Alabama at Birmingham, SHEL 803, 1825 University Blvd, Birmingham, AL 35294, USA.
Email: yhsong@uab.edu

Erik D. Roberson, Alzheimer's Disease Center, Center for Neurodegeneration and Experimental Therapeutics, & Departments of Neurology and Neurobiology, Marnix E. Heersink School of Medicine, University of Alabama at Birmingham, SHEL 1171, 1825 University Blvd, Birmingham, AL 35294, USA.
Email: eroberson@uabmc.edu

Funding information
National Institutes of Health, Grant/Award Numbers: T32GM008361, T32NS095775, T32EB023872, R01AG068395, R01AG081228, P20AG068024; Alzheimer's of Central Alabama; Alzheimer's Drug Discovery Foundation; Alzheimer's Association, Grant/Award Number: AARG-16-441560; BrightFocus Foundation, Grant/Award Number: A2022032S; National Science Foundation, Grant/Award Number: OAC-1541310; University of Alabama; Alabama Innovation Fund

Abstract

INTRODUCTION: The immune receptor triggering receptor expressed on myeloid cells 2 (TREM2) is among the strongest genetic risk factors for Alzheimer's disease (AD) and is a therapeutic target. TREM2 multimers have been identified in crystallography and implicated in the efficacy of antibody therapeutics; however, the molecular basis for TREM2 multimerization remains poorly understood.

METHODS: We used molecular dynamics simulations and binding energy analysis to determine the effects of AD-associated variants on TREM2 multimerization and validated with experimental results.

RESULTS: TREM2 trimers remained stably bound, driven primarily by salt bridge between residues D87 and R76 at the interface of TREM2 units. This salt bridge was disrupted by the AD-associated variants R47H and R98W and nearly ablated by the D87N variant. This decreased binding among TREM2 multimers was validated with co-immunoprecipitation assays.

DISCUSSION: This study uncovers a molecular basis for TREM2 forming stable trimers and unveils a novel mechanism by which TREM2 variants may increase AD risk by disrupting TREM2 oligomerization to impair TREM2 normal function.

KEYWORDS
Alzheimer's disease–associated variants, binding free energy analyses, experimental validation, molecular dynamics simulations, oligomerization, TREM2

Hunter B. Dean and Rory A. Greer contributed equally to this study.

- -

Highlights

- Triggering receptor expressed on myeloid cells 2 (TREM2) multimerization could regulate TREM2 activation and function.
- D87–R76 salt bridges at the interface of TREM2 units drive the formation of stable TREM2 dimers and trimers.
- Alzheimer's disease (AD)–associated R47H and R98W variants disrupt the D87–R76 salt bridge.
- The AD-associated D87N variant leads to complete loss of the D87–R76 salt bridge.

1 | BACKGROUND

Heterozygous genetic variants in the innate immune receptor triggering receptor expressed on myeloid cells 2 (TREM2) have been associated with multiple neurodegenerative diseases, including Alzheimer's disease (AD).[1-6] Most clinically relevant variants such as R47H are thought to directly impair TREM2's ability to bind ligands and transduce their signals, by preventing TREM2 maturation and localization to the cell surface,[7] decreasing electrostatic potential at the basic surface patch immediately around R47,[8] or allosterically disrupting stability of the complementarity-determining region (CDR)–like loops, which underly an apical patch of hydrophobic residues.[9,10] However, several AD-associated variants retain surface expression and show some ability to bind ligands and transmit signal to TREM2's intracellular binding partners DNAX-activating protein of 12 kDa (DAP12) and/or DNAX-activating protein of 10 kDa (DAP10).[11-14]

One possible effect of AD-associated variants is on TREM2 multimerization. Crystal structures of the common variant (CV) human TREM2 immunoglobulin domain with (PDBID: 6B8O) or without (PDBID: 5UD7) phosphatidylserine (PS) show TREM2 molecules packing in a homo-hexameric arrangement (Figure 1A). This hexamer consists of a densely packed inner trimer, where each member is loosely associated with one outer TREM2 molecule.[9] Analyses of shape complementarity and buried solvent-accessible surface area suggest that the outer three TREM2 molecules are not likely to be strongly associated with the inner trimer, and are more likely to be an artifact of crystallization. This is consistent with asymmetric units in other crystal structures that show pairs of unassociated TREM2 monomers in a tail-to-tail conformation.[8] In contrast, the inner trimer shows shape complementarity and buried solvent-accessible surface area, which are more similar to interacting multimers.[9] D87 is located in the trimer's interacting surface, suggesting that D87 may play a role in stabilizing this interaction. Although the effect of D87N on TREM2 multimerization has not been studied, TREM2 containing the R47H variant crystalizes primarily as monomers.[9] In addition, although the CDR loops that are disrupted by TREM2 AD-associated variants directly underly the apical hydrophobic patch, the beta sheets that maintain CDR stability underlie the trimer interface,[9,10] providing a possible structural mechanism by which AD-associated variants may reduce the propensity of TREM2 to multimerize.

There are indications that TREM2-activating antibodies currently in development as AD therapeutics act by inducing TREM2 multimerization, and the valence of the crosslinking may regulate the level of activation. Monoclonal antibodies and crosslinked antibody fragments that divalently engage TREM2 can induce phosphorylation of the downstream kinase Syk, mobilize intracellular calcium, and prevent cleavage of TREM2's extracellular domain by secretases, whereas monovalent engagement of TREM2 with fragments of the same antibodies does not.[15-17] Furthermore, monoclonal TREM2 antibodies engineered with four variable domains activate TREM2 in reporter lines at more than a 100-fold lower concentration than divalent antibodies.[18] Notably, in addition to reducing amyloid beta (Aβ) pathology and behavioral deficits in 5xFAD mouse models of AD,[19] antibody-induced activation of TREM2 can overcome survival and migration deficits caused by the R47H variant in mouse macrophages.[20] Altogether, evidence from antibodies suggest that the valence of multimerization may play a key role in regulating TREM2-dependent intracellular signaling, and that targeting the multimerization of TREM2 may be a viable method for improving therapeutics for both sporadic and TREM2 variant–associated AD.

These observations suggest that TREM2 multimerization may contribute to its function, but little is known about the structural basis of TREM2 multimerization, including the minimum number of TREM2 molecules required to form a stable multimer or how TREM2 multimerization may be affected by AD variants. We examined the structure of TREM2 multimers using classical molecular dynamics (MD) simulations and binding free energy analysis, followed by experimental validation with co-immunoprecipitation. Results from this study identify a novel loss-of-function mechanism for variants in TREM2, demonstrate stability of both trimers and dimer conformations of TREM2, and have implications for TREM2-targeting therapeutics currently in development for neurodegenerative diseases.

2 | METHODS

2.1 | TREM2 model generation and mutagenesis

The initial hexameric model for this study of the immunoglobulin domain of CV human TREM2 bound to PS was obtained from a 2.2 Å

crystal structure (PDBID: 6B8O). Five of the six chains in this crystal structure have a small region missing from the crystal structure, mostly at a motile loop near residues 54–58. We first reconstructed the missing region for each of the five chains based on the complete chain A structure in crystal structure (PDBID: 6B8O) using homology modeling, by aligning the complete chain A sequence (residues 21–129) with each of the remaining TREM2 molecules with the homology modeling software package MODELLER.[21] The completed hexamer structure was then energy minimized by steepest descent followed by conjugate gradient using AMBER14.[22] Trimer and dimer models of TREM2 were isolated from this initial hexamer as chains A, B, and C (trimer) or chains A and D (dimer) with associated PS ligands (Figure 1A). The trimer structures containing the R47H, D87N, R98W, P37D, or G90D variants in each TREM2 and the trimer structures containing the R47H variant in only one TREM2 were generated by mutating the corresponding residues from the isolated trimer model using the mutagenesis tool in PyMOL (Figure 1B).[23] For each mutated residue, the orientation with the fewest predicted steric clashes was selected as the starting orientation. We additionally generated models of CV TREM2 at pH levels of 6.4, 7.4, and 8.4 using the equilibrated structures of CV TREM2 with the PDB2PQR and PROPKA[24,25] in the APBS-PDB2PQR software suite.[26] Each of the finalized multimer models was then globally energy minimized by steepest descent followed by conjugate gradient in AMBER14 for pilot studies of multimer stability,[22] or AMBER18 for characterization of the trimers with variants[27] to obtain starting structures for the MD simulations. For the pilot studies, histidine residues were assumed to be fully protonated (HIP in AMBER) to minimize the effects of surface charge that might displace PS at the examined timescales, while triplicate simulations for variant analysis were run with the histidine unprotonated (HIE in AMBER), which is more likely to be present at cell-surface pH levels. The models generated at pH levels of 6.4, 7.4, and 8.4 were protonated as determined by the PDB2PQR program with PROPKA.

2.2 | Surface electrostatic potential and hydrophobicity

Maps showing the electrostatic potential and hydrophobicity were generated to show the locations of relevant ligand binding sites in the minimized TREM2-CV multimer model. Electrostatic potential was mapped using the Adaptive Poisson-Boltzmann Solver[26] package in PyMOL.[28] Hydrophobicity was assigned using a modification of the *color_h* script in PyMOL, which assigns color values by residue based on the Eisenberg hydrophobicity scale.[29]

2.3 | MD simulation setup

MD simulations were performed with AMBER14 for pilot studies of multimer stability or AMBER18 for characterization studies of the

RESEARCH IN CONTEXT

1. **Systematic review**: Using traditional sources (i.e., peer-reviewed journal articles, PubMed) the authors reviewed the available literature, which supports the importance of multimerization for the activation and function of triggering receptor expressed on myeloid cells 2 (TREM2). However, the number of TREM2 subunits needed to form a stable multimer, the molecular mechanisms for multimer formation, and the effects of AD-associated variants on TREM2 multimerization are not well understood.

2. **Interpretation**: Our computational studies identified key interactions between subunits in TREM2 multimers and showed that AD-associated variants could either reduce (R47H and R98W) or completely block (D87N) these interactions. These findings were validated with experiments showing decreased TREM2 multimerization by TREM2 R47H or D87N variants.

3. **Future directions**: This combined computational and experimental approach can help to address additional hypotheses and questions in future studies. Examples include (1) the molecular basis of other disease-associated TREM2 variants on TREM2 multimerization and (2) the effects of small molecules as TREM2 ligands on TREM2 multimerization.

trimers with variants, using the ff14SB force field for both.[30] Each MD simulation was performed in a periodic box with 2 nm of solvent, consisting of TIP3P water and Na^+ and Cl^- ions at 0.15 M and random starting positions, between the outer edge of the protein and the box boundary to reduce the periodicity artifacts. Additional ions of Na^+ or Cl^- were added to the periodic box with AMBER's *addions2* algorithm to neutralize the charge of the TREM2 models. After the solvated protein systems were set up, we ran steepest descent minimization followed by a 20 ps constant number-pressure-temperature (NPT) equilibration step of the water solvent, both with the TREM2 trimer and ions restrained. To heat the system to 300 K we ran a series of 10 ps constant number-volume-temperature (NVT) MD simulations at 50, 100, 150, 200, 250, and 300 K. After the simulations were heated, we set up MD production simulations (250 ns per model for pilot stability studies; 500 ns per model in triplicate for CV, R47H, R98W, and D87N trimer characterization studies; or 500 ns per model for P37D and G90D trimer studies), at constant NPT of 300 K and 1 bar. Electrostatic interactions were calculated by the particle-mesh Ewald method, and Lennard–Jones cutoffs were set at 1.0 nm. All MD simulations used SHAKE constraints with a relative tolerance of 1×10^{-5} on each hydrogen-heavy atom bond to allow for accelerating the simulations using 2 fs time steps.
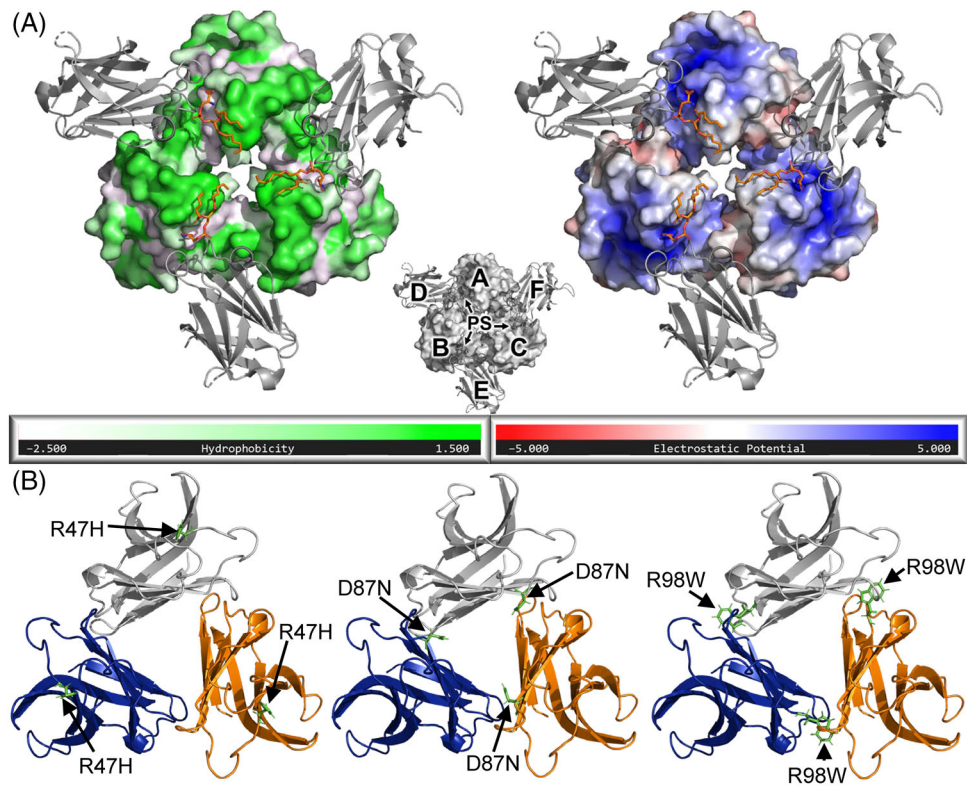
FIGURE 1 Models of TREM2-R47H, TREM2-D87N, and TREM2-R98W trimers for molecular dynamics simulations. (A) Positions of the two previously described ligand binding sites of TREM2 from the initial hexameric structure. In this trimer model, the hydrophobic patch is oriented toward the center of the trimer (shown in green on the left) and the basic path is oriented away (shown in blue on the right). The lipid ligand phosphatidylserine (orange) crystalizes in an orientation with its head group toward the basic patch and its tail toward the hydrophobic. The letters used in this manuscript to distinguish the six different TREM2 molecules contained in each hexamer model are diagrammed in the middle. (B) TREM2 trimer showing the locations of the mutated residue generated using PyMOL for the R47H, D87N, or R98W variant in each of the three TREM2 molecules. The well-characterized R47H variant is distal from the interaction interface, whereas both R98W and D87N occur in or near the interface.

2.4 | Steered MD simulation

To further evaluate the effects of AD-associated variants R47H and D87N on TREM2 multimerization, we implemented steered MD (SMD) simulations with a constant-velocity protocol to probe the dissociation of one subunit from the rest of the trimer for CV TREM2 trimer along with the R47H and D87N variants. We used the NAMD 2.12 MD package[31] for SMD simulations, and the Amber force field was used for the systems. The equilibrated models from repetition 1 of CV, repetition 1 of R47H variant, and repetition 1 of D87N variant were globally energy minimized by steepest descent followed by conjugate gradient to obtain the starting structures for the SMD simulations. The structures were solvated, the solvent minimized and then equilibrated, and finally the system was heated to 300 K as described in the preceding MD simulation setup section. As described in our previous study,[32] SMD simulations were used to probe the effects of R47H and D87N variants on TREM2 multimerization. A constant pulling speed of 0.2 Å/ps was applied to each alpha carbon of each residue on the beta sheets of pulled TREM2 subunit. The residues in the other two subunits, except the residues in the binding interface with the pulled subunit, were treated as rigid and fixed. The pulling direction was along

the center of mass of both the pulled and fixed residues. Equation 1[33] determines the force experienced by the alpha carbon atoms of the pulled residues:

$$F = K(vt - x) \tag{1}$$

F is force, K is the spring constant, set as 7 kcal/mol/Å^2, v is the pulling velocity, set as 0.2 Å/ps, t is time, and x is the movement of the pulled alpha carbon atom from its original position. We averaged the three force extension profiles for each variant from the three subunits (i.e., subunit A to B and C, subunit B to A and C, and subunit C to A and B) to generate the average force extension profile for each variant. The average force extension profiles for the CV, R47H, and D87N variants were compared to determine how the AD-associated variants affected TREM2 multimerization.

2.5 | Equilibration and dissociation analysis

To determine the equilibration and convergence of the simulated systems, we calculated the root mean square deviation (RMSD) of the

backbone alpha carbon atoms of the individual TREM2 molecules within the multimers over time; the RMSD of the backbone alpha carbon atoms of the entire TREM2 multimer over time; and the distance between the centers of mass of the TREM2–TREM2 binding sites within the trimer over time. Centers of mass were defined using atoms from all contacting residues in the TREM2 molecules on either side of the interaction based on the energy-minimized CV model. Based on these analyses and the convergence of molecular mechanics Poisson Boltzmann surface area (MM-PBSA) binding free energy analysis below, we determined the initial simulation time needed for each simulation to reach system equilibration and used the simulation trajectories after the equilibration point for further analyses of structure, dynamics, and binding affinity.

To identify any events where a molecule of TREM2 completely dissociates from the rest of the complex, we used the molecular mechanics Poisson Boltzmann surface area (MM-PBSA) method,[34,35] as described later, to calculate binding enthalpy between the three TREM2 molecules during the MD simulation, as calculated enthalpy should be zero whenever any molecule of TREM2 loses contact with the rest of the complex. However, because the trimers have two binding sites per molecule, to identify events where only a single interacting site within the trimer dissociates or where one TREM2 molecule shifts its interaction to a novel site on its partner, we measured distances between the centers of mass for each interacting surface. For this, we also defined any frame from the trajectory where the initial interacting surfaces shifted by more than 25 Å as a dissociation event from the initial site, regardless of whether the molecules completely dissociated or just shifted to a new interacting interface.

2.6 | Binding free energy analysis

The binding free energy for all models was calculated with the MM-PBSA method, which was implemented using AMBER14 for pilot studies of multimer stability or AMBER18 for analysis of the trimers with variants.[34,35] The MM-PBSA method combines molecular mechanics, continuum electrostatics, and solvent-accessible surface area calculations for enthalpy, with the option to include normal mode harmonics analysis for entropy estimation, to calculate the binding energies from a series of snapshots obtained from the MD trajectories.

In the MM-PBSA method, binding free energy of a receptor–ligand complex can be calculated as the difference between the enthalpy and entropy (Equation 2), where ΔG_{bind} is binding free energy, ΔH is enthalpy, T is temperature, and ΔS is entropy. The enthalpy (ΔH) can be calculated as the sum of the molecular mechanics contribution (ΔE_{MM}) and the solvation free energy (ΔG_{solv}) of the system (Equation 3). The molecular mechanics contribution (Equation 4) is made up of the sum of the intermolecular van der Waals energy (ΔE_{vdw}), intermolecular electrostatic energy (ΔE_{elec}), and internal energy (ΔE_{int}). The internal energy (Equation 5) is made up of the energy resulting from bond (ΔE_{bond}), angle (ΔE_{angle}), and torsion energies ($\Delta E_{torsion}$), as well as the van der Waals ($\Delta E_{1-4\ vdw}$) and electrostatic ($\Delta E_{1-4\ elec}$) energies between atoms separated by three bonds (a dihedral angle).

The solvation free energy term is made up of both polar (ΔG_{polar}) and nonpolar components ($\Delta G_{nonpolar}$) (Equation 6). The polar contribution is calculated with the Poisson-Boltzmann equation and is based on the electrostatic contribution to solvation. The nonpolar contribution comes from the cavity formation in the solvent. Finally, the entropy component is made up of contributions from translational motion (ΔS_{trans}), rotational motion (ΔS_{rot}), and vibrational motion (ΔS_{vib}) calculated using normal mode analysis (Equation 7).

$$\Delta G_{bind} = \Delta H - T\Delta S \qquad (2)$$

$$\Delta H = \Delta E_{MM} + \Delta G_{solv} \qquad (3)$$

$$\Delta E_{MM} = \Delta E_{vdw} + \Delta E_{elec} + \Delta E_{int} \qquad (4)$$

$$\Delta E_{int} = \Delta E_{bond} + \Delta E_{angle} + \Delta E_{torsion} + \Delta E_{1-4\ vdw} + \Delta E_{1-4\ elec} \qquad (5)$$

$$\Delta G_{solv} = \Delta G_{polar} + \Delta G_{nonpolar} \qquad (6)$$

$$\Delta S = \Delta S_{trans} + \Delta S_{rot} + \Delta S_{vib} \qquad (7)$$

The change of any energy component of a system can be calculated from the individual components of the complex (Equation 8), where $\bar{G}$ is the average energy value of the trajectory.

$$\Delta G = \bar{G}_{complex} - \bar{G}_{protein} - \bar{G}_{Ligand} \qquad (8)$$

In the case of our system, the complex was assumed to be the entire multimer (including PS, when present), the protein was the single TREM2 molecule whose binding energy to the rest of the trimer we were calculating, and the ligand was the other two TREM2 molecules as well as any PS ligands present. To calculate all the terms of the enthalpy contributions, we used snapshots of the entire trajectory at a time interval of 100 ps for pilot studies of multimer stability or 150 ps for analysis of the trimers with variants. Due to the high computational costs of the entropy calculations, we used snapshots at a 1.5 ns interval for the normal mode analysis used in the entropy calculation.

Although more precise equations for predicting the equilibrium binding constant K_{eq} based on simulated free energy changes have been reported,[36] the classical approximation (Equation 9), where k_B is the Boltzmann constant and C_0 is a reference concentration of 1 mol/L, was sufficient to estimate the relative changes in binding caused by inclusion of the AD-associated variants in this study.

$$\Delta G_{bind} = -k_B T \ln(K_{eq} C_0) \qquad (9)$$

2.7 | Inter-residue distances and correlated motion

To identify changes in binding site locations or large rearrangements within individual TREM2 molecules, we measured pairwise distances between alpha carbons from each residue for every model. To analyze correlated motions between residues of interest, we generated a dynamic cross-correlation map (DCCM) between alpha carbons for each TREM2 model over the equilibrated trajectory, the equations for which we have described in detail previously.[10] In DCCM maps, each residue pair is ultimately assigned a value between −1 and 1, where

−1 is assigned to pairs of residues that have perfectly anticorrelated motion in space, 1 is assigned to pairs with perfectly correlated motion, and 0 is assigned when the two residues move independently. Distances and DCCM were measured for each residue pair at every frame of the equilibrated portion of the trajectory, and an N × N matrix of RMS averaged values was generated for each model. To remove artifact effects caused by individual TREM2 molecules shifting relative to each other in space, each column of the DCCM map is aligned to a different single TREM2 molecule, resulting in the appearance of vertical red stripes at residues from adjacent TREM2 molecules that are strongly pulled by motion of the aligned TREM2 molecule. Both maps show intramolecular interactions in the regions along the diagonals.

2.8 | Conformational flexibility

To identify changes in flexible motions of the protein backbone, we examined root mean square fluctuations (RMSFs) at each amino acid. RMSF was calculated using centers of the alpha carbons of each TREM2 residue over the equilibrated portion of the simulation trajectory. For pilot studies, RMSFs are presented separately for each TREM2 molecule to allow comparisons between models containing a mix of TREM2-CV and TREM2-R47H molecules.

2.9 | Secondary structure

To determine the percentage of equilibrated frames that each residue spent as a β-strand, α-helix, 3_{10}-helix, or unstructured strand, bend, or loop, we assigned secondary structures per residue at each frame using the define secondary structure of proteins (DSSP) method in AMBER's *cpptraj* module,[37] which calculates based on an idealized (i.e., assuming 1.000 Å from the backbone N opposite the backbone C = O bond) hydrogen bond energy using all nearby atoms. The energies from the two most favorable hydrogen bonds are then compared to those of all secondary structures for protein models stored in the RCSB Protein Database to assign the most likely secondary structure for that residue. These calculations are performed for each equilibrated frame over the MD simulation and presented as a percentage of frames in the equilibrated trajectory that the residue occupies a particular secondary structure.

2.10 | Energy decomposition analysis

To identify key residues involved in the binding of the TREM2 trimer, we used energy decomposition of the enthalpy components of binding. Energy decomposition is a way to decompose the enthalpy term (excluding nonpolar solvation energy) into its individual components to identify which residues have the strongest contribution to energy changes in the binding. Energy decomposition was performed in trimer models using AMBER18 for each of the three TREM2 molecules sep-

arately, to determine which residues contributed most toward that molecule's total enthalpy of binding.

2.11 | Salt bridge occupancy analysis

To calculate the percentage occupancy of a salt bridge between arginine 76 of one TREM2 molecule to aspartate 87 of another molecule (or of a hydrogen bond between R76 and the uncharged N87 in TREM2-D87N models, a salt bridge between arginine 98 and aspartate 37 in the TREM2-P37D model, or a salt bridge between arginine 98 and aspartate 90 in the TREM2-G90D model), we determined the percentage of frames in the entire equilibrated trajectory where at least one hydrogen bond existed between the two residues. A hydrogen bond was assigned when the donor heavy atom and acceptor were less than 3 Å apart and the angle was no less than 135°. For analysis of salt bridge occupancy over time, the percentage of frames containing the bond was calculated within nonoverlapping 1 ns segments, rather than within the entire equilibrated trajectory.

2.12 | Clustering analysis

Clustering analysis was performed on the equilibrated portions of the trajectories to help visualize a representative structure for each simulation. For simulations except TREM2-D87N repetition 2 and TREM2-D87N repetition 3, we performed clustering analysis of the last 250 ns of trajectory to identify the representative structures of the simulations. For TREM2-D87N repetitions 2 and 3, we used the 50 ns immediately prior to the dissociation event to identify the representative pre-dissociation structures and the last 150 ns of the simulation to identify the representative post-dissociation structures. The *dbscan* (density-based spatial clustering of applications with noise) algorithm was input with structural coordinates from the isolated portions of each trajectory and allowed to cluster frames that share similar structural features, as described previously.[10] To determine the parameters of the *dbscan* clustering algorithm and minimize the bias for each simulation, we generated K-distribution plots (at $K = 5$) to determine a minimum informative distance cutoff between clusters. Once run, the *dbscan* algorithm generates a representative frame that most closely represents the average structure for the primary cluster, which we used for representation and further analysis.

2.13 | Cell culture and co-immunoprecipitation

HEK-293T cells (#CRL-3216, ATCC) were cultured in DMEM (Corning Life Sciences) with 10% fetal bovine serum (Atlanta Biologicals) and 1% penicillin/streptomycin (ThermoFisher) at 37°C and 5% CO_2. Cells were transiently transfected using FuGENE HD Transfection Reagent (Promega) with a plasmid expressing full-length human TREM2 with an N-terminal HA-tag and/or an N-terminal FLAG-tag inserted after the signal peptide.[8] TREM2 constructs were either CV, R47H, or D87N,

and both the HA- and FLAG-tagged TREM2 had the same variant in each transfection. After 72 h, the cells were harvested in lysis buffer (50 mM Tris, 150 mM NaCl, 5 mM EDTA, 1% Triton X-100, 0.1% sodium deoxycholate) and centrifuged 5 min at 3000 × g. Lysate containing 150 μg of total protein was diluted to 250 μL with lysis buffer and precleared with 25 μL of Protein G Dynabeads (ThermoFisher) for 30 min at 4°C. Tagged TREM2 was immunoprecipitated using 25 μL of fresh Protein G Dynabeads with 2.5 μg of anti-HA tag antibody (mouse monoclonal [F-7], #sc-7392, Santa Cruz Biotechnology) or 2.5 μg of anti-DYKDDDDK antibody (rabbit monoclonal [D6W5B], #14793, Cell Signaling Technology). Immunoprecipitates and sample lysates were run on 4-12% bis-tris polyacrylamide gels (ThermoFisher), transferred to Immobilon-FL PVDF (MilliporeSigma), blocked for 1 h with Pierce Protein-Free (TBS) Blocking Buffer (Thermo Scientific), and probed overnight with primary antibody (either anti-HA at 1:1000 or anti-FLAG at 1:1000) containing Quick Western IRDye 680RD Detection Reagent (Li-COR Biosciences), which minimizes nonspecific signal from the denatured antibody light chains because it does not bind denatured mouse monoclonal or rabbit monoclonal antibodies. Primary antibodies to distinguish the differentially tagged TREM2 for the western blot were the same as those used for the immunoprecipitation: anti-HA (mouse monoclonal [F-7], #sc-7392, Santa Cruz Biotechnology) or anti-DYKDDDDK (rabbit monoclonal [D6W5B], #14793, Cell Signaling Technology).

For testing TREM2 multimerization at different pH levels, the HEK-293T cells were transfected with both the HA- and FLAG-tagged versions of TREM2-CV. After 48 h, cells were harvested and lysed using lysis buffers of different pH values (pH 6.4, 7.4, or 8.4). IP was performed in lysis buffers of the corresponding pH values using anti-HA tag antibody for overnight at 4°C. The immunoprecipitates and sample lysates were run on a 11% polyacrylamide gel (Fisher Science) and transferred to a nitrocellulose membrane (Bio-Rad). Membranes were blocked with 5% non-fat milk and incubated with primary anti-HA (1:1000 dilution) or anti-DYKDDDDK (1:1000 dilution) overnight at 4°C. After the membranes were washed three times with 1× TBST, membranes were incubated with horseradish peroxidase-conjugated secondary antibodies (donkey anti-mouse (Southern Biotech 6410-05) diluted 1:10,000 for anti-HA primary antibody and donkey anti-rabbit (Southern Biotech 6440-05) diluted 1:10,000 for anti-DYKDDDDK primary antibody) for 1 h at room temperature. Signals were detected using ECL western blotting substrate.

2.14 | Native PAGE

HEK-293T cells were transfected with vectors expressing FLAG-tagged TREM2-CV. Forty-eight hours after transfection, cells were harvested for non-denaturing polyacrylamide gel electrophoresis and western blot analysis (native PAGE). Briefly, cells were lysed with ice-cold cell lysis buffer (20 mM, pH 8.0 Tris, 137 mM NaCl, 1% Triton X 100, and 2 mM EDTA). The total protein concentration of cell lysates was measured with a Pierce BCA protein assay kit (Thermo Scientific). Cell lysates with equal amounts of protein were mixed with 3× sam-

ple loading buffer (240 mM Tris-HCl pH 6.8, 30% glycerol, and 0.03% bromophenol blue) and kept on ice (not heated). Samples were loaded into 10% native polyacrylamide gel wells. Gel electrophoresis was performed at 4°C using a running buffer without sodium dodecyl sulfate (SDS). The proteins in the gel were transferred to a nitrocellulose membrane. Membranes were blocked with 5% non-fat milk and incubated with primary antibody rabbit anti-DYKDDDDK (1:1000 dilution) antibodies overnight at 4°C. The membranes were washed three times with 1× TBST and then incubated with horseradish peroxidase-conjugated secondary antibodies (donkey anti-rabbit diluted 1:10,000) for 1 h at room temperature. Signals were detected using ECL western blotting substrate.

2.15 | Statistical analysis and technical specifications

For trimer characterization models run in triplicate and presented in aggregate (including binding energies, RMSF, enthalpy decomposition, DCCM, and inter-residue distance maps), values are presented as averages of all nine TREM2 molecules (i.e., three points each over three replicate simulations for nine points per residue) unless otherwise stated.

The mean and standard error of each component of the binding free energy over the equilibrated portion of the trajectory was calculated by bootstrapping mean values from randomly isolated, statistically independent intervals along the trajectory, according to a method we have described previously.[10] For TREM2-CV, TREM2-R47H, and TREM2-R98W models, contributions from all nine TREM2 molecules (i.e., three points each over three replicate simulations for nine points total and 250 ns each) were used for determining bootstrap parameters. For dissociating TREM2-D87N models, bootstrap parameters were generated using only the TREM2–TREM2 interactions present during analysis (e.g., pre-dissociation trajectories are considered to have three bonds present and are examined for 50 ns, whereas post-dissociation trajectories have only one bond remaining and are examined for 150 ns).

Means comparisons for this study were performed using analysis of variance (ANOVA) with a 95% confidence interval (CI), followed by Tukey HSD post hoc analysis for comparison between variants or pH values. All statistical tests and data visualizations were performed using R 4.2.1.[38]

3 | RESULTS

3.1 | TREM2 multimers are identified in cell lysate

Before analyzing whether AD-associated variants could affect TREM2 multimerization, we needed to determine which TREM2 multimer conformations could stably form. As stated earlier, crystal structures of TREM2 appear to show a hexameric arrangement; however, there is only loose association in those models between a closely associated

inner TREM2 trimer and the three outer TREM2 molecules. To determine whether multimers of TREM2 form outside of crystallography experiments, we generated HEK-293T cells expressing a construct containing CV human TREM2 (TREM2-CV). We ran lysates from these cells on non-denaturing polyacrylamide gel electrophoresis (native PAGE) and blotted for TREM2 (Figure S1). Although it is difficult to directly equate the predicted sizes on native PAGE gels due to the lack of SDS providing a consistent charge distribution, the blot revealed three clear bands in the TREM2-CV transfected lane, suggesting that at least some multimer species of TREM2 are present. If the three bands of ≈30, 55, and 80 kDa are assumed to correlate with TREM2 bands in SDS-PAGE gels, this would likely represent monomers, dimers, and trimers of TREM2, respectively. Notably, there were no clear bands between 80 kDa and a large smear near the 200 kDa range. This suggests that larger multimers of TREM2, such as the proposed hexamer, did not form in significant proportions in this experiment, but that there may be multiprotein complexes bound to TREM2 or nonspecific aggregates of TREM2 present in the solution.

3.2 | Stability of TREM2 dimers

Based on the multiple bands in native PAGE, we next sought to identify conformations of TREM2 multimers that are likely to exist stably in solution. For example, tail-to-tail dimer conformations of TREM2 have been identified in multiple crystals; however, because they have few close intermolecular interactions and low buried solvent accessible surface area in the initial crystal structure, these dimers are thought to be an artifact of the crystallization and unlikely to exist in solution.[8,9] To address this, we initiated a set of MD simulations derived from the hexamer crystal structure described earlier, isolating two molecules: TREM2-CV in a tail-to-tail dimer conformation generated using one TREM2 molecule from the inner trimer and its associated outer TREM2 molecule (Figure S2A).

To determine whether individual TREM2 molecules equilibrated during the simulation, regardless of the conformation of the whole complex, we first examined the RMSD of the alpha carbons from each molecule separately. Although the two individual TREM2 molecules within the CV/CV dimer reached equilibration quickly by RMSD (Figure S2B), the CV/CV dimer model dissociated quickly within the first 5 ns of simulation (Figure S2C; dashed red line), suggesting that this tail-to-tail TREM2 dimer conformation is not stable at the observed timescales. Notably, after falling apart and reforming in multiple possible configurations over the first 50 ns, the dimer eventually found a different tail-to-tail conformation with more favorable binding enthalpy (Figure S2B–C). Measuring the distance from the center of masses for the interacting interfaces reveals that following the dissociation events, the final stable binding site found by the dimer was the same binding interface used by the inner TREM2 trimer in the starting crystal structure (Figure S2D). Notably, when this interface forms, it appeared to consistently do so around a salt bridge utilizing the residue D87, which was bound in the same portions of the trajectory that developed favorable binding enthalpy (Figure S2E). These results show that the

specific tail-to-tail dimer identified in crystal structures is unstable at sub-microsecond timescales, but that multimers of TREM2 can form around a salt bridge that seems to be driven by the residue D87.

In previous crystallography experiments, soaking the crystals in the TREM2 ligand PS appeared to increase the size and shape complementarity of the contacting interfaces in the TREM2 multimer, which may imply a stabilizing effect of PS or may simply be driven by crystal packing artifacts.[9] To examine whether addition of PS would cause TREM2 to more readily form this dimer conformation or increase the dimer's affinity, we re-ran the simulation, this time including the PS molecule present in the original crystal structure. The addition of PS did not significantly stabilize the trajectory, with MM-PBSA results showing the dimer again falling apart multiple times early in the trajectory and failing to find a strongly stable conformation (Figure S2C). The addition of R47H variants to either or both molecules of TREM2 when bound to PS also failed to stabilize the dimers at the R76-D87 salt bridge, supporting the original finding that these variants would, if anything, destabilize TREM2. Altogether these results suggest that neither the binding of single molecules of PS nor introduction of the R47H variant is able to stabilize the TREM2 dimer conformations previously described in crystallography. Although this study does not rule out the possibility that some other stable dimer conformation exists such as those seen by native PAGE (Figure S1), experimental methods would be needed to better characterize the location of the interacting interface before they could be more fully explored in MD simulations.

3.3 | Stability of TREM2 trimers

Based on the presence of the stabilizing D87 salt bridge in its starting structure, we next examined the stability of the inner TREM2-CV trimer isolated from the same crystal structure (Figure S3A) using a set of 250 ns MD simulations. We again used RMSD to confirm equilibration of the individual TREM2 molecules, followed by MM-PBSA analysis to identify dissociation of the complex. RMSD revealed little change for the CV/CV/CV trimer across the 250 ns trajectory (Figure S3B). Similarly, for the CV/CV/CV trimer as a whole, the binding interface remained stable throughout the trajectory without any dissociation events observed by either loss of binding enthalpy (Figure S3C) or increase in binding site distance (Figure S3D), suggesting that this symmetric trimer conformation was stable enough for further analysis of the effects of AD-associated variants or ligand binding.

To examine whether inclusion of the R47H variant would destabilize the trimer conformation, as predicted in previous studies, we mutated one or all three molecules of TREM2-CV to TREM2-R47H and re-ran the MD simulations. We have previously described a conformational shift in TREM2-R47H monomers, which is visible by RMSD and driven by motion at the loops underlying the hydrophobic and multimerization sites.[10] Unsurprisingly, some of the individual TREM2-R47H molecules showed this increase in RMSD across the trajectory, particularly in the TREM2-A molecule of the R47H/R47H/R47H model (Figure S3B). The increase in RMSD in this model is driven primarily by untethering of the β-sheet consisting of residues 68–74 underlying CDR2, which can

be seen as loss of secondary structure (Figure S3E), increased flexibility (Figure S3F), conformational changes in the associated loops (Figure S3G), and changes in correlated motion (Figure S3H) in this region. However, although small shifts were seen in the binding sites, particularly in the TREM2-A–TREM2-B sites of both R47H-containing models, neither showed a complete dissociation event in the examined time period by either MM-PBSA or site distance analysis (Figure S3C,D), suggesting that the intramolecular effects of R47H may affect binding affinity, but are not sufficiently severe to completely disrupt the complex at these timescales. In addition to using MM-PBSA to help define dissociation events, we also used the calculated binding enthalpies over the equilibrated portion of the trajectory to examine how R47H affected binding affinity for each complex. As predicted, inclusion of the R47H variant decreased binding enthalpy in proportion to the number of TREM2 molecules containing the variant (Figure S3I).

To again examine whether a stabilizing ligand such as PS could improve the binding affinity of the trimer, we ran simulations of TREM2 trimers containing the same sets of variants, but this time including three PS molecules, one bound to each molecule of TREM2. Overall, adding PS had little effect on the stability of individual molecules of TREM2 or the binding affinity of the CV/CV/CV-PS trimer (Figure S3B–I). It is surprising that PS may even further disrupt trimerization when R47H is present, as R47H/CV/CV-PS and R47H/R47H/R47H-PS both dissociated during the simulations (Figure S3B–D), although it is difficult to determine whether this was driven by the PS or simply a rare dissociation event driven by R47H that happened to be captured in these models but not the two lacking PS. Altogether the R47H-dependent loss of affinity in these pilot studies, combined with the lack of a stabilizing effect from PS, suggested that a closer inspection of trimer models containing other environmental effects or AD-associated variants might reveal more about the mechanisms at play in TREM2 trimerization.

3.4 | Effects of pH value on TREM2 multimerization

We next asked whether changes in specific environmental factors, such as pH, may affect the stability of TREM2 trimers. To do so, we used PDB2PQR[26] to calculate the protonation state of each residue within the equilibrated TREM2-CV trimer at a local pH of 6.4, 7.4, or 8.4 (Figure S4A). Using this method, when the pH was raised to 8.4, residue C36 deprotonated in all three subunits, adding a negative charge to each binding interface and causing the overall electrostatic surface potential of the interface to become more negative (Figure S4B). In contrast, at a pH of 6.4, residues H103 and H114 had a propensity to protonate, with four of the six histidine residues from each model becoming protonated. Although the protonation of H114 had little effect on the electrostatic surface potential of the TREM2, the protonation of H103 shifted the electrostatic surface potential at this residue from slightly negative/neutral to positive (Figure S4C). Using the MM-PBSA method to predict changes in binding enthalpy at the different pH levels, we found that as pH increased, the binding enthalpy

became stronger, driven primarily by favorable electrostatic interactions at the binding interface (Figure S4D). When pH was lowered to 6.4, the binding enthalpy weakened by 4.3 kcal/mol, and when pH was raised to 8.4, the binding enthalpy strengthened by −3.1 kcal/mol compared to a pH of 7.4 (Figure S4E).

To validate these computational predictions, we utilized a co-immunoprecipitation (co-IP) assay to measure the effects of pH on TREM2 multimerization. To do so, we generated constructs expressing full-length human TREM2 tagged with either an HA or FLAG tag just after the N-terminal signal peptide. We then co-transfected these constructs in HEK-293T cells and immunoprecipitated just the HA tag from lysates with an HA-specific antibody. This immunoprecipitate was then blotted for the presence of both peptide tags, to determine whether molecules of TREM2 containing the HA tag could pull down molecules of TREM2 containing FLAG, indicating formation of a TREM2 multimer. As predicted, when lysates from cells co-transfected with HA-tagged and FLAG-tagged common variant TREM2 were pulled down with antibodies to HA, FLAG could be detected by western blot (Figure S4F), confirming that the tagged molecules of common variant TREM2 multimerized in vitro. When the same experiment was carried out at pH 6.4, TREM2 multimerization decreased, whereas at pH 8.4, TREM2 multimerization increased (Figure S4F–G), consistent with the computational results. These findings could indicate that TREM2 multimerization may be less favorable in the slightly more acidic environment of aging and Alzheimer's disease brains.[39] In addition, these results further validate that TREM2 multimers can be found in vitro and that computational predictions about the stability of TREM2 multimers correlate well with experimental results.

3.5 | Residue D87 is required for TREM2 to maintain stable trimers

After our initial simulations suggested that TREM2-CV could form stable trimers that were affected by the R47H variant and by local charge, we wanted to further explore how AD-associated variants would affect trimer stability, binding energy, and intermolecular interactions. To examine these effects, we set up new MD simulations wherein all three TREM2 molecules were mutated to the same variant of interest: CV, R47H, D87N, or R98W (Figure 2A; see Experimental Procedures for simulation setup). Each model was run to at least 500 ns in triplicate to increase sampling of potential dissociation events that may occur more rarely or over a longer timescale.

After the 12 simulations (four variants with three repetitions each) were completed; four metrics were measured for each to determine whether the trajectories reached equilibration as intact trimers: RMSD of individual TREM2 molecules within the trimer over time, RMSD of the entire trimer complex over time, distance between each of the three binding sites within the trimer measured over time with centers again defined using the contacting residues in the energy minimized TREM2-CV model, and the MM-PBSA enthalpies between each TREM2 molecule as the receptor and remaining pair of molecules as the ligand over time (Figure 2B–M). Again, we defined dissociation
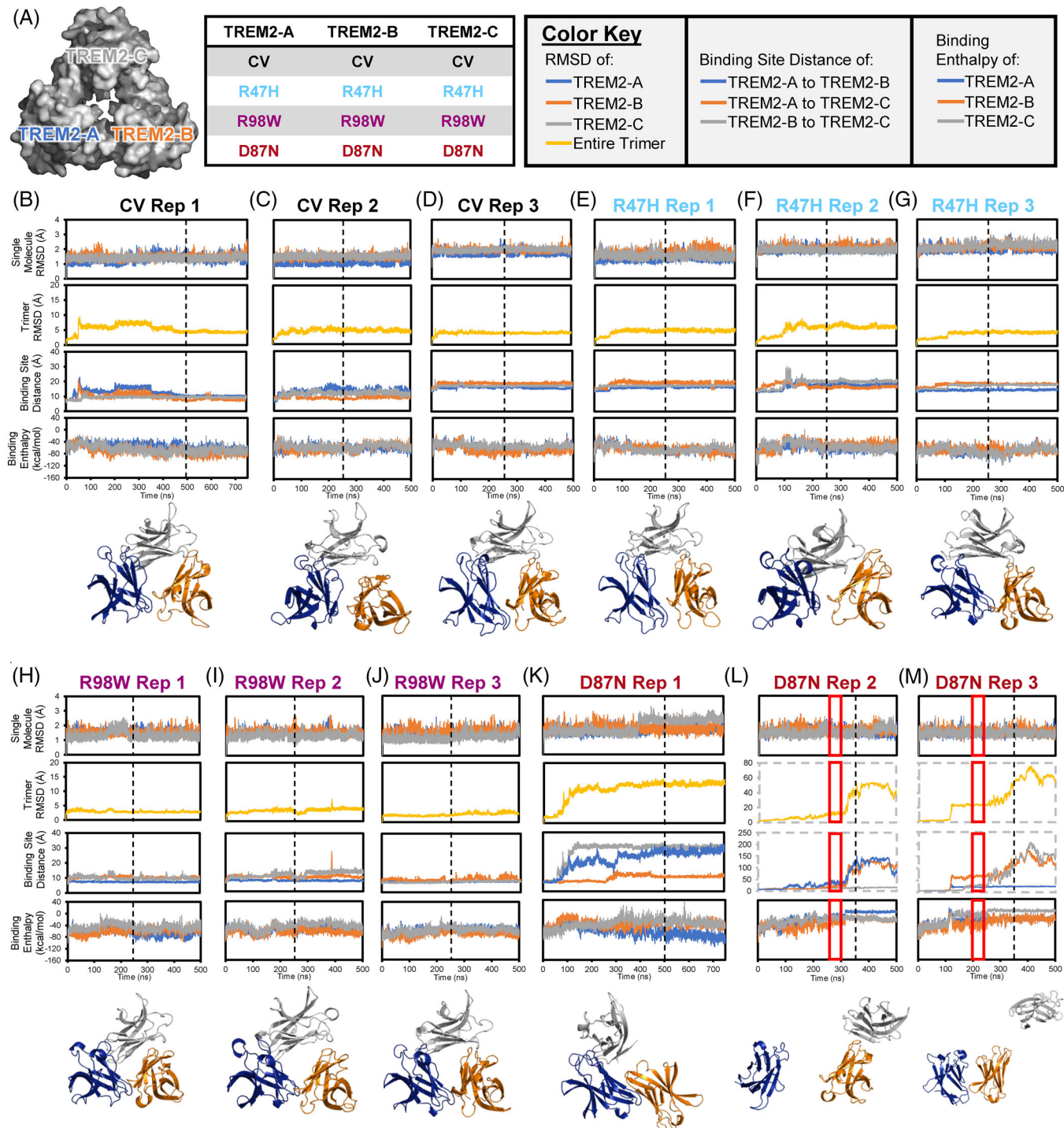
FIGURE 2 The AD-associated D87N variant abolished TREM2 trimerization. (A) Experimental design for the MD simulations in this figure. Triplicate simulations using models of TREM2-CV trimers, of TREM2-R47H trimers, of TREM2-R98W trimers, and of TREM2-D87N trimers were run in MD simulations for at least 500 ns. (B–M) Equilibration metrics for each MD simulation show that, of the examined AD-associated variants, only D87N tends to cause complete dissociation of multimers in our models. Shown for each simulation are (from top to bottom) the RMSD of the alpha carbons for each residue in the three separate TREM2 molecules, RMSD of the alpha carbons for each residue in the entire trimer together, the distance between centers of mass for the three biding sites, the frame-by-frame enthalpy values over time, and the representative structure from the equilibrated portion of the trajectory. The structures for repetitions 2 and 3 of TREM2-D87N show the first isolated frame where TREM2-A (repetition 2) or TREM2-C (repetition 3) is completely dissociated from the other two molecules of the trimer. Vertical dashed lines show the start point of the equilibrated 250 ns (150 ns for D87N repetitions 2 and 3) used for downstream analysis of each simulation. Red boxes show the 50 ns immediately before complete dissociation of the D87N trimer that are isolated for "pre-dissociation" analysis in Figure 4. Dashed gray outlines are used for panels that share an extended y-axis. RMSD, root mean square deviation.

events as occurrences where at least one TREM2 molecule dissociated from the complex entirely (i.e., its binding enthalpy went above zero) or where at least one starting binding interface was disrupted without the complex completely dissociating (i.e., the binding site center of mass distance rose above 25 Å for more than 5 ns).

By these metrics, the RMSD of the individual TREM2 molecules revealed no large conformational changes within each model, except a single stepwise increase in one molecule of TREM2 from repetition 1 of the TREM2-D87N model (Figure 2K). There were no dissociation events in any of the CV, R47H, or R98W simulations. However, all of the D87N simulations had trimer dissociation events. D87N repetition 1 had large shifts in its binding interfaces (Figure 2K) but did not completely dissociate, whereas TREM2-A of repetition 2 (Figure 2L) and TREM2-C of repetition 3 (Figure 2M) both fell away from the remaining pair of molecules completely. In both cases, the two remaining TREM2 molecules appeared to retain a dimer for the remainder of the simulation, albeit with a significantly lower binding affinity than seen in the trimeric state. In addition, two of the simulations failed to equilibrate within the initial 500 ns for the minimum 250 ns that we had set as analyzable time: TREM2-CV repetition 1 (Figure 2B) and TREM2-D87N repetition 1 (Figure 2K). These two simulations were run for an additional 250 ns to ensure that all models—except for the two TREM2-D87N models that completely dissociated—had at least 250 ns of equilibrated time for further analysis (shown in Figure 2 following black, vertical dashed lines). The two TREM2-D87N models with complete dissociation events were instead analyzed by isolating the last 150 ns of the intact dimer (shown in Figure 2 following black, vertical dashed lines) and the 50 ns prior to the dissociation event (shown in Figure 2 within a red box) to examine the changes occurring during dissociation.

3.6 | Effects of AD-associated variants R47H and R98W on TREM2 trimers

Because neither R47H nor R98W caused the trimer to completely dissociate, we further analyzed the equilibrated last 250 ns of their trajectories to determine the effects of these variants on the stability and binding affinity of the trimer (Figure 3A). As a more precise estimate of the effects of each variant on the total binding affinity of the trimer, we used MM-PBSA for enthalpy estimation and normal-mode analysis of harmonic frequencies for entropy estimation to give an overall measure of binding free energy. Each of the enthalpy and entropy terms was calculated per molecule by subtracting the energy contributions of a single TREM2 molecule (i.e., the receptor) and the remaining pair of TREM2 molecules (i.e., the ligand) from the energy of the overall complex. Per-molecule values were then averaged across all nine examined TREM2 molecules from each variant, three from each model (Figure 3B, Figure S5). Binding analysis showed that TREM2-CV had the most negative (i.e., highest affinity) binding free energy, with the TREM2-R47H and TREM2-R98W models both having about 2 kcal/mol lower affinity when the variants were present. Due to the log scale relationship between binding free energy and the number of interacting

molecules, this $\approx$2 kcal/mol decrease equates to an $\approx$40 times decrease in predicted equilibrium binding constant, that is, a > 95% decrease in the number of TREM2–TREM2 interactions that would be found in solution at equilibrium.

To identify the mechanism by which the variants decreased the trimer binding affinity, we first looked at RMSF to determine whether the lower binding affinity was likely caused by altered conformational stability within individual TREM2 molecules. Plots showing the average RMSF for all nine molecules from each variant model (Figure 3C) revealed that R47H had little effect on conformational stability compared to TREM2-CV, whereas R98W weakly destabilized all three loops underlying the hydrophobic site, most notably the third loop at residues 88–90.

In the absence of a large conformation change to explain changes in binding affinity caused by R47H and R98W, we then looked for localized surface effects that might explain the binding affinity changes. For this, we looked at per-residue decompositions of the binding enthalpies from MM-PBSA analysis to determine if contributions of particular residues to binding were affected consistently by the variants. Averaging the energy contributions from the nine TREM2 molecules containing each variant (three each in three repetitions) revealed two residues, R76 and D87, as having the greatest negative (i.e., favorable for binding) contribution in TREM2-CV, with smaller peaks at P37, W78, and N99 (Figure 3D).

To further confirm that D87 and R76 are key residues involved in trimerization of TREM2, we compared the inter-residue distances and dynamic cross-correlation maps (DCCM) for each variant. Inter-residue distance maps showed that the pattern of close contacts at the binding interfaces in red were not largely changed between variants, with the D87 to R76 distance notable as a dark red dot in each binding site (Figures 3E and G, solid boxes). However, distance maps only suggest proximity and do not necessarily show binding interactions between any residue pair. In contrast, the DCCMs, in which vertical red bands between two TREM2 molecules indicate residues on the centered molecule that are pulled when the correlated molecule moves, showed differences between the correlated motions of TREM2 molecules within the trimer (Figure 3F,G). In particular, vertical bands representing interactions at R76 (dashed boxes) and D87 (dotted boxes) were dark red in each subunit of the TREM2-CV model (Figure 3G), showing that interactions between the matched molecules were highly correlated at these residues. R47H or R98W variants caused a decrease in correlated motion between R76 or D87 and the corresponding TREM2 molecules, suggesting that these residues may play a key role in the TREM2 trimer's ability to remain in a bound state (Figure 3F,G).

We then asked how these residues may control the binding affinity change caused by AD-associated variants. When looking more closely at the trimer structure, it is evident that R76 and D87 form a salt bridge between neighboring molecules of TREM2 (i.e., TREM2-A D87 with TREM2-C R76, TREM2-B D87 with TREM2-A R76, and TREM2-C D87 with TREM2-B R76; Figure 3H). Closer examination of the total enthalpy contributions of each residue (Figure 3D) revealed that D87 was more heavily affected by the variant models than its major binding
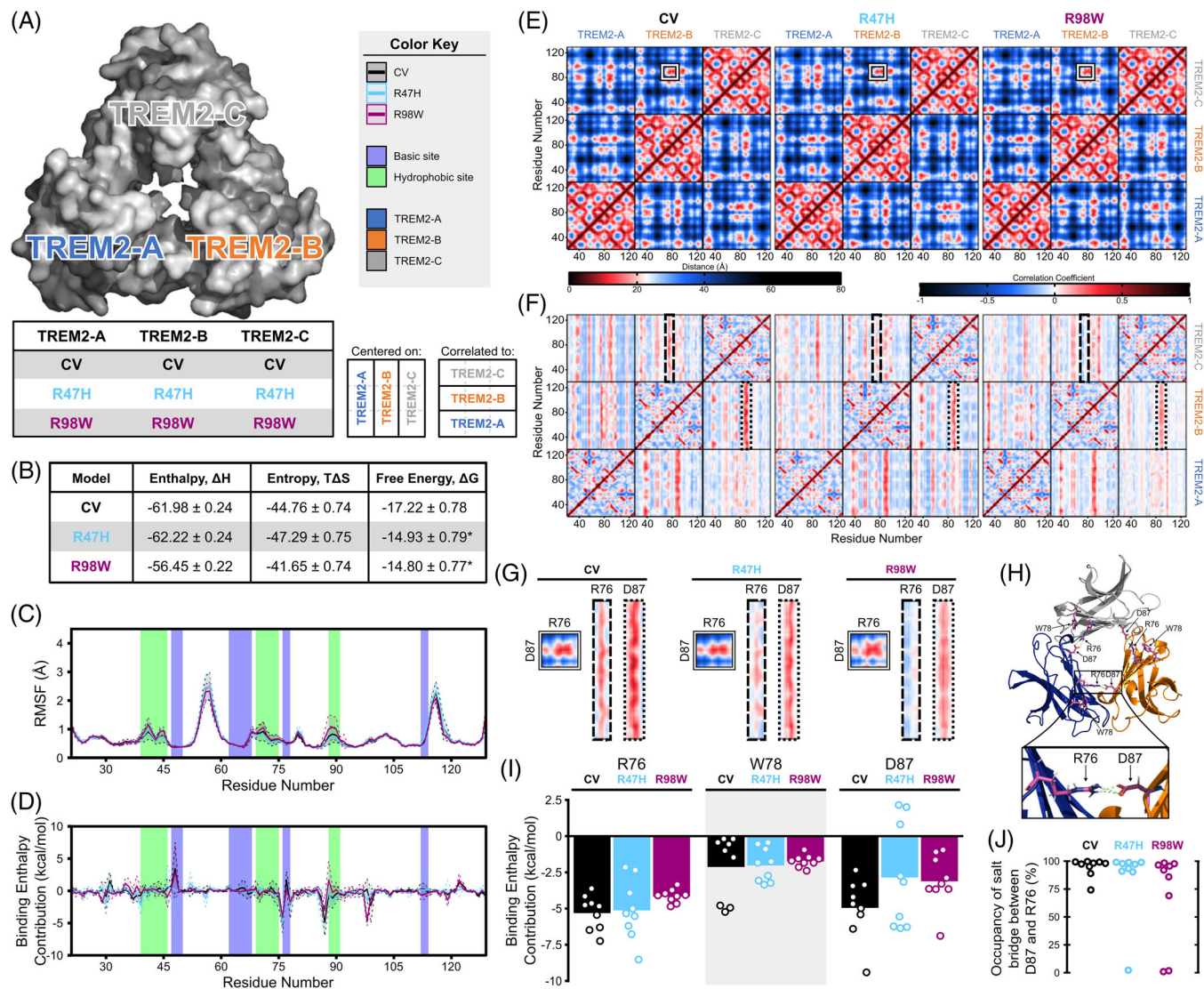
FIGURE 3 The AD-associated R47H and R98W variants allosterically disrupt key interactions in TREM2 trimers and reduce the binding energies of the TREM2 molecules. (A) Experimental design for the MD simulations compared in this figure. (B) Calculated enthalpies, entropies, and free energies of binding for each TREM2 trimer model showing decreased affinity in the models containing AD-associated variants. Values are shown as mean ± standard error for the equilibrated trajectories of all nine TREM2 molecules for each variant (i.e., three molecules from three simulations each). *$p < 0.05$ in comparison to TREM2-CV by Tukey post hoc analysis. (C) Comparison of average RMSFs of the TREM2 molecules between TREM2-CV, TREM2-R47H, and TREM2-R98W trimers show small, localized differences in conformational stability between models. (D) Comparison of the decomposed enthalpy contribution of each residue between TREM2-CV, TREM2-R47H, and TREM2-R98W trimers shows that decreased affinity is driven by a small number of interactions at key residues including R76 and D87. (E) Inter-residue distance maps show small or no changes in the overall conformation between TREM2-CV, TREM2-R47H, and TREM2-R98W trimers, including at residues R76 and D87. (F) DCCM maps show that R47H or R98W mutations in all three TREM2 molecules alter intra- and intermolecular correlated motion, particularly with respect to residues R76 and D87. (G) Example insets from (E) and (F) showing that although the distance between the residues does not change between variants (solid boxes), by DCCM the motion of R76 from subunit B becomes less correlated with subunit C (dashed boxes) and, similarly, D87 from subunit C becomes less correlated with subunit B (dotted boxes) when the AD-associated variants are present. (H) TREM2-CV trimer representative structure showing R76 and D87 form a salt bridge between TREM2 molecules. (I) Comparison of the enthalpy contribution from (D) focusing on R76, W78, and D87 show that the loss of affinity in the TREM2-R47H and TREM2-R98W trimers is driven largely by D87. (J) Average salt bridge occupancy between D87 and R76 for the TREM2-CV, TREM2-R47H, and TREM2-R98W trimers shows that the salt bridge is lost in a small number of interactions when the AD-associated variants are present. DCCM, dynamic cross-correlation map.

partner R76 or its minor partner W78, with the total enthalpy contributions of D87 decreased by roughly half in each variant (Figure 3I). This ≈2 kcal/mol change in binding enthalpy closely matches the total change in free energy caused by these variants (Figure 3B), suggesting that the decreased binding seen in these variants may be driven almost entirely by their effects on binding at D87. Finally, looking at the percent occupancy of this salt bridge across the equilibrated portion of the trajectory, it is evident that models of TREM2-CV had >70% occupancy in all R76-D87 salt bridges between the three repetitions, with >95% occupancy in all but two (Figure 3J). In contrast, TREM2-R47H and TREM2-R98W had multiple R76-D87 salt bridges with lower occupancy, suggesting lower overall stability at this bond, with at least one salt bridge lost in each. Notably, these low-occupancy bonds occurred on one or both sides of the same TREM2 molecules that showed the lowest affinity in MM-PBSA analysis: TREM2-B–TREM2-C from repetition 2 of the TREM2-R47H model, TREM2-B–TREM2-C from repetition 1 of TREM2-R98W, and TREM2-C–TREM2-A from repetition 2 of TREM2-R98W (Figure S5). These results suggest that that a salt bridge between R76 and D87 plays a key role in stabilizing TREM2 trimers, and that the effects of both R47H and R98W on TREM2 trimerization are driven, at least in part, by their effects on binding at this salt bridge.
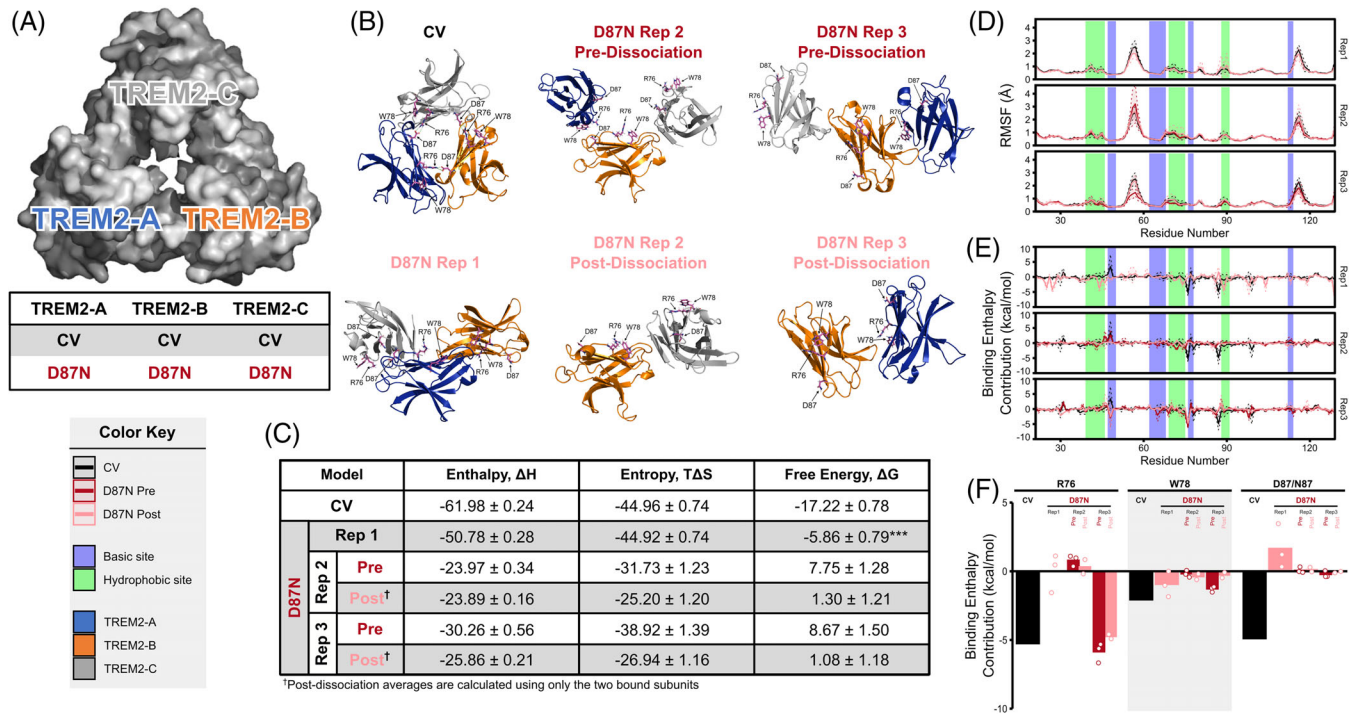
3.7 | The AD-associated D87N variant prevents key intermolecular interactions in the TREM2 trimer

Given that TREM2-R47H and TREM2-R98W both appear to impair binding through their effects at a salt bridge involving D87, it was clear that mutation of D87 from aspartate, a charged residue, to asparagine, a neutral residue, may have caused the trimers to dissociate (Figure 2K–M) through loss of the same salt bridge. To confirm this prediction and to determine whether the incompletely dissociated repetition 1 model, or the remaining dimers in repetitions 2 or 3, was likely to remain as a stable complex, we examined the last 250 ns from TREM2-D87N repetition 1 as well as the 50 ns windows immediately prior to complete dissociation of the trimer and the last 150 ns of the post-dissociation trajectories from TREM2-D87N repetitions 2 and 3 (Figure 4A). Post-dissociation values were calculated from only the two remaining TREM2 molecules in the dimer. By 50 ns prior to complete dissociation, TREM2-D87N repetitions 2 and 3 had already lost major interactions near the original salt bridge, with R76, W78, and N87 not continuing to be bound to the adjacent TREM2 molecule (Figure 4B). In addition, although repetition 2 still utilized N87 and R76 as interacting residues, it no longer maintained any of the key interactions from the TREM2-CV trimer binding site (Figure 4B). Furthermore, binding free energy analysis showed that D87N reduced the binding affinities of the TREM2 molecules within the trimer (Figure 4C). Although TREM2-D87N repetition 1 found a stable binding site, it was much lower affinity than any of the other examined variants, R47H or R98W. In contrast, repetitions 2 and 3 showed that introducing the D87N variant was highly unfavorable for binding, with even the post-dissociation periods having positive free energies, suggesting that even

the remaining dimers would not be predicted to stay together beyond the examined trajectory. Similarly, taking the time-averaged contribution of all examined interacting surfaces from the TREM2-D87N models gives an overall binding free energy of near zero, suggesting that even the appearance of transient low-affinity interactions is likely not sufficient to maintain stable TREM2–TREM2 interactions over these timescales.

To further determine whether the effects of D87N were due solely to the loss of its salt bridge with R76 or whether there were any contributions from loss of conformational stability of the individual TREM2 molecules or binding at other regions, we again examined the RMSF and per-residue binding enthalpy decomposition. Except for one highly mobile loop near residues 55–58, there was little notable change in the RMSF (Figure 4D). Per residue decomposition across all three repetitions showed a loss of binding enthalpy contribution from the major binding residues present in TREM2-CV (Figure 4E), especially at the mutated N87 (Figure 4F). Instead, TREM2-D87N repetitions 1 and 3 showed small contributions from many residues distributed across the surface, whereas repetition 2 showed almost no strong interactions (Figure 4E). Both patterns are consistent with the TREM2-D87N models exploring possible surface interactions nonspecifically following loss of the stable binding site. Similar patterns of non-specific changes between the three models were seen in inter-residue distance maps and DCCM (Figure S6). Altogether, the lack of either major conformational changes or appearance of any consistent novel interactions between the TREM2-D87N models, indicates that loss of the R76-D87 salt bridge is sufficient to disrupt any ability of TREM2 to maintain a stable trimer conformation.

It is notable that in the above MD simulations, the D87N variant was able to fully dissociate one subunit over the course of the simulation, whereas the R47H variant caused a decrease in binding energy but not complete dissociation. This is likely due to the limited timescale of classical MD simulations, as the R47H variant would likely need more time for its allosteric effects to completely propagate through the TREM2 molecule as opposed to D87N, which directly breaks a key binding interaction between subunits. To further examine whether the R47H variant could affect TREM2 trimer association, we utilized steered MD (SMD) simulations to determine how D87N and R47H affected the force required to break the binding of one subunit from the other two subunits in the trimer (Figure S7A). Utilizing constant velocity, we pulled each subunit away from the other two subunits in the trimer (i.e., subunit A from B and C, subunit B from A and C, and subunit C from A and B). By observing the reaction force by the pulling, we could identify when the pulled subunit began to dissociate, as a significant increase of reaction force by pulling indicates the breaking of the binding between subunit of trimer. The average peak force required to break apart the CV TREM2 trimer (≈3000 pN) was much stronger than the average peak force required to break apart the R47H or D87N variant trimers (≈2000 pN), (Figure S7B). These results further verify that both R47H and D87N variants can reduce TREM2 multimerization to similar degrees when their effects are made to be less time-dependent, with both variants requiring similar levels of force to break the trimer apart.

FIGURE 4 D87 is a necessary residue for TREM2 multimerization that is impaired by the AD-associated D87N variant. (A) Experimental design for the MD simulations compared in this figure. Because D87N repetitions 2 and 3 dissociated, we separately examined the 50 ns immediately prior to dissociation (Pre) and the last 150 ns of the equilibrated trajectory (Post). (B) Representative structures for the TREM2-CV and TREM2-D87N trimer models with the dissociated models shown as both pre- and post-dissociation structures. (C) Binding free energy of the TREM2 molecules for each TREM2-CV and TREM2-D87N repetition, both pre- and post-dissociation for repetitions 2 and 3, showing the loss of affinity in the TREM2-D87N models. Values are shown as mean ± standard error for the equilibrated portions of all nine TREM2 molecules for each variant (i.e., three molecules from three simulations each) or for the one remaining bond in post-dissociation trajectories. ***$p < 0.001$ in comparison to TREM2-CV by Tukey post hoc analysis. (D) Comparison of average RMSFs of the TREM2 molecules between TREM2-CV trimers and TREM2-D87N trimers, both pre- and post-dissociation for repetitions 2 and 3, show that changes in binding affinity are not associated with large changes in conformational flexibility. (E) Comparison of the average total enthalpy contribution of each residue between TREM2-CV and TREM2-D87N, both pre- and post-dissociation for repetitions 2 and 3. (F) Comparison of the total enthalpy contribution from (E) focusing on R76, W78, and D87/N87 for both models (pre- and post-dissociation for TREM2-D87N), shows that changes in overall binding affinity are driven primarily by loss of interactions at D87. CV, common variant.

3.8 | Engineered TREM2 P37D and G90D variants increase TREM2 multimerization

If AD-associated variants could reduce TREM2 multimerization by disrupting a salt bridge between subunits, we hypothesized that mutations engineered to add another salt bridge in the same interface could increase TREM2 multimerization. Along with residue R76, there is a second arginine nearby in the binding interface, R98. We looked for residues near R98 on the opposing subunit that could be mutated to an aspartic acid to form a second salt bridge at this residue. From observing the binding interface, we identified both residues P37 and G90 as potential candidates to mutate to aspartic acid to form this second salt bridge (Figure S8A). In a manner similar to the AD-associated variants, both P37D and G90D variants were allowed to run 500 ns MD simulations. Equilibration was determined to have occurred before 250 ns by RMSD of the individual subunits, RMSD of the trimer, the change in distance between the binding interfaces, and the binding enthalpy (Figure S8B,C). Representative structures of both P37D and G90D variants

confirmed that the trimers could form double salt bridges between the subunits (Figure S8B,C). To further investigate the degree of formation of these double salt bridges between the subunits, we determined the salt bridge occupancy between R76 and D87 as well as the salt bridge occupancy between R98 and either D37 (P37D variant) or D90 (G90D variant). Both P37D and G90D variants caused the occupancy of the salt bridge between R76 and D87 to decrease (Figure S8D), replaced in part by the new salt bridge between the mutated residue and R98. Notably, the G90D variant had a higher occupancy of the new salt bridge with R98 compared to P37D (Figure S8E). The difference in the double salt bridge occupancy between G90D and P37D likely explains at least in part why the G90D variant nearly doubled the binding free energy of the TREM2 trimer compared to CV, whereas the P37D variant modestly increased the binding free energy only modestly (Figure S8F). These findings confirm the importance of salt bridging at the subunit interface for stability of the TREM2 trimer and highlight the potential use of these engineered mutations of TREM2 to better study the role of TREM2 multimerization in AD.
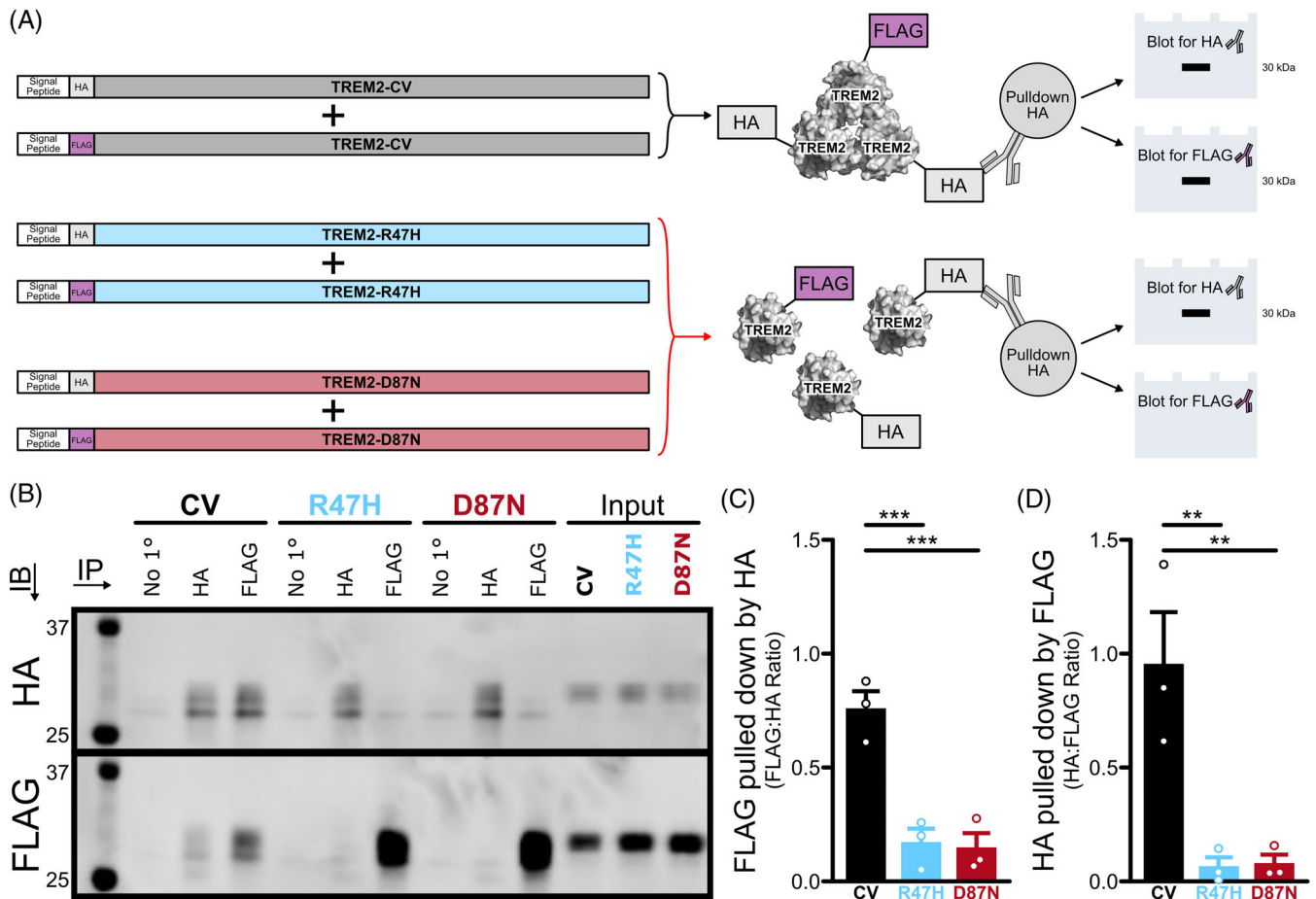
FIGURE 5 AD-associated variants R47H and D87N impair TREM2 multimerization in vitro. (A) Experimental design for co-immunoprecipitation experiments in this figure. Constructs containing the same variant were generated with either an HA or FLAG tag and transfected into HEK-293T cells. The tag of interest was immunoprecipitated from the lysate, and antibodies specific to both tags were used to IB. Immunoprecipitation of TREM2 constructs that multimerize should yield bands immunoreactive with both tags, whereas immunoprecipitation of TREM2 constructs with impaired multimerization should yield primarily bands immunoreactive with the tag pulled down and less of the other tag. (B) Representative images of co-immunoprecipitations of TREM2-CV, TREM2-R47H, or TREM2-D87N tagged with either HA or FLAG show the expected pattern, with bands for the pulled down tag visible for all, but bands of the non-targeted tag lost in the lanes containing AD-associated variants. (C, D) Quantification of three independent experiments like that shown in (B). Pulldown efficiencies are calculated as the ratio between the tag that was not pulled down by immunoprecipitation (FLAG in C, HA in D) over the tag that was pulled down (HA in C, FLAG in D). $n = 3$ independent transfections and pull-downs per group, $^{**}p < 0.01$, $^{***}p < 0.001$. IB, immunoblot. IP, immunoprecipitation.

3.9 | Experimental validation of R47H and D87N effects on TREM2 multimerization

To confirm our in silico predictions that AD-associated variants in TREM2 could impair its multimerization, we again utilized a co-IP design using constructs expressing full-length human TREM2 tagged with either an HA or FLAG tag (Figure 5A). We co-transfected these constructs in HEK-293T cells, this time immunoprecipitating either the HA or FLAG tag from lysates with specific antibodies. This immunoprecipitate was then blotted for the presence of the two peptide tags. As before, when lysates from cells co-transfected with HA-tagged common variant TREM2 (HA-TREM2-CV) and FLAG-tagged common variant TREM2 (FLAG-TREM2-CV) were pulled down with antibodies to either tag, the other tag could be detected by western blotting (Figure 5B–D), confirming that the tagged molecules of com-

mon variant TREM2 multimerized in vitro. In contrast, immunoblots of pulldowns from co-transfections of HA- and FLAG-tagged TREM2-R47H or of HA- and FLAG-tagged TREM2-D87N primarily contained the pulled-down tag, not the corresponding co-transfected tag (Figure 5B–D), confirming that these AD-associated variants inhibit multimerization of TREM2 in a cell-based model.

4 | DISCUSSION

In this study we describe a trimeric form of TREM2 that is stable in MD simulations. We identify a salt bridge between D87 and R76 as the key interaction stabilizing this trimer and show that acidic environments and AD-associated variants—including R47H, D87N, and the putative AD-associated variant R98W—all weaken this interaction, whereas

variants engineered to introduce additional salt bridges nearby can strengthen it. We also show that asymmetric dimers isolated from the same crystal structures are not stable under the same conditions, but that a stable dimer conformation may be able to form if the R76-D87 salt bridge is present. Finally, we provide biochemical validation of the computational findings by showing that AD-associated variants R47H and D87N disrupt TREM2 multimerization in cells.

Our study adds impaired multimerization to the list of potential mechanisms for TREM2 loss-of-function caused by the R47H variant, alongside electrostatic disruption at the charged patch surrounding R47, allosteric destabilization of the loops underlying TREM2's apical hydrophobic site, and decreased TREM2 maturation and surface localization, among others.[8–10] Notably, the effects of R47H on trimerization do not seem to be a direct result of instability in the CDR loops, as this instability was identified in only a subset of the trimer models and was not required for loss of binding affinity between molecules of TREM2 in these models. Although we limited our focus here to variants directly in the multimerization site (D87N and R98W) along with the strongly AD-associated R47H variant, future work may benefit from examining other variants near this site but not directly involved in the multimer interface, such as the AD-associated R62H or FTD-associated D86V variants, which we have shown previously to have intramolecular structural effects similar to R47H,[10] or the K48M mutation, which has been used in previous studies as a engineered null mutation and is believed to form a stabilizing internal salt bridge with D86.[14] In addition, although mutations in R76 have not previously been reported to be associated with disease, it is notable that the only reported variants at this locus in the Genome Aggregation Database, GnomAD, are either synonymous or mutations to the similarly charged amino acid lysine, raising the possibility that genetic variants that mutate R76 into non-basic residues are not well tolerated in humans.[40]

Although multimerization has been shown to play a role in TREM2 activation by antibodies as discussed in the introduction, its role in TREM2 signaling in vivo is not yet known. Multimerization has been described previously as a necessary step for intracellular signaling in the closely related TREM1[41] and is a common step in ligand and signal transduction for many subclasses of receptors including toll-like receptors,[42] tumor necrosis factor (TNF) receptors,[43] and other lipoprotein-binding receptors.[44,45] Thus it is likely that impairments in TREM2's ability to form multimers may lead to an associated loss of TREM2 signaling. AS the endogenous ligand(s) of TREM2 remain elusive, and as binding residues for the majority of TREM2's known ligands have only recently started to be elucidated,[46] it is difficult to interrogate whether multimerization is required for binding of certain ligands or whether it is an important step in transducing certain intracellular signals. However, because single molecules of PS had only modest effects on multimerization in our simulations, and because TREM2 is known to bind both small molecule[11,47–49] and protein ligands[12,13,46,50] as well as larger lipid and lipoprotein particles[14,51] and oligomerized peptides including Aβ,[46,52,53] it is possible that crosslinking through multivalent engagement by large or aggregated ligands represents a mechanism by which certain ligands

induce different activation states of TREM2. This stepwise activation by higher affinity ligands has been described in other immunoreceptor tyrosine-based activation motif (ITAM)-associated receptors[54,55] and proposed in commentaries as a method by which TREM2 may differentially activate two of its downstream signaling pathways, with high-affinity or multivalent ligands recruiting the kinase Syk in the canonical TREM2-DAP12 pathway, while lower-affinity or monovalent ligands act through an alternative pathway independently of Syk, potentially through DAP10.[56,57]

Preferentially disrupting multimerization while leaving some amount of alternative signaling intact could also explain how certain disease variants in TREM2 seem to be loss-of-function in some models but incomplete loss or even gain-of-function in others. For example, the D87N variant, although rare in the general population, has previously given conflicting results in binding and signaling studies. D87N does not appear to grossly alter TREM2's folding, promote its aggregation in assays using recombinant protein, or prevent its surface localization,[8] which is consistent with a loss-of-function mechanism that occurs at or downstream of initial ligand engagement. At the same time, despite decreasing TREM2's ability to bind lipoprotein particles in cell-free assays,[14] D87N does not decrease TREM2-dependent uptake of lipidated apoJ,[14] and even leads to increased signal transduction when TREM2 is activated by purified phospholipids, high-density lipoprotein (HDL), or low-density lipoprotein (LDL) in reporter cells.[49] Because the functional relevance of TREM2 multimerization is still unclear, it is possible that apparent decreases in binding in cell-free assays are driven by a loss of multimerization-dependent recruitment of additional TREM2 molecules, but that this multimerization is not required to induce some intracellular signaling in simplified cell models and may even reduce signaling by certain lower-affinity ligands.

The simulations in this study utilize only the extracellular immunoglobulin domain of TREM2 and do not account for any contribution from the transmembrane region or connecting stalk, suggesting that the general mechanisms of multimerization described herein may be able to occur in both membrane-bound and soluble forms of the receptor. Soluble forms of TREM2 have been found to act as signaling molecules, but their receptor remains unknown. If this multimerization mechanism is, in fact, independent of the isoform of TREM2, it is even possible that soluble TREM2 may act as a ligand for membrane-bound forms of TREM2, forming mixed-isoform multimers that could aid in signaling or inhibit binding of other ligands.

Future studies may also benefit from more thoroughly examining the effects of variant heterozygosity on the formation, stability, or even signaling properties of TREM2 multimers. In human population, most carriers of disease-associated variants in TREM2 are heterozygous, carrying one copy of the disease-associated variant and one copy of the common variant. This means that any particular multimer of TREM2 formed in the body of a heterozygous carrier could possibly contain any combination of the two variants. In the example of a person who is heterozygous for the R47H variant, this means that four different species of trimer could be present in some proportion throughout the body: those containing zero, one, two, or three molecules of TREM2-R47H. This study shows preliminary evidence that incorporating even

a single molecule of R47H into TREM2 trimers causes an intermediate degree of disruption to the trimer's overall binding affinity (Figure S3I). However, it is unclear from structural studies alone whether the presence of a disease-associated variant would primarily affect signaling throughout the body by simply diluting the number of TREM2-CV molecules available to form high-affinity multimers, by sequestering some molecules of TREM2-CV into non-functional multimers containing other molecules of the variant TREM2, or by some other method such as recruitment of an alternative signaling partner like DAP10, as discussed earlier.

This study is also limited in the same way as all studies that use simplified in silico and in vitro models to address complex biological questions. Our work utilizes multimer conformations identified in x-ray crystallography, correlates well with the effects of variants and ligands noted using that approach, and is supported by biochemical assessment of multimerization. On the other hand, our simulations use assumptions such as an already intact trimer and limited timescales, which gives trimers the advantage of already being in an optimal binding conformation and having less than a microsecond for interactions to weaken. In contrast, in a bulk system such as the human body, decreased binding affinity would primarily cause trimers to fail to form in the first place, rather than to preferentially dissociate as occurs in our model. This means that the 2 kcal/mol decrease in affinity caused by R47H (Figure 3B), which is already sufficient to decrease the number of TREM2–TREM2 interactions by >95%, may actually underestimate the decrease in binding caused by the variant when it is found in unbound monomers of TREM2 in the body. This, alongside the incomplete propagation of allosteric changes at limited MD timescales, may also explain why TREM2-R47H multimers are not seen even at very low levels in experiments such as our co-immunoprecipitation or previous studies of TREM2 using x-ray crystallography, which are often not sufficiently sensitive to detect log-scale decreases in prevalence. Thus this work will still require further validation in biophysical experiments in order to more precisely measure the binding affinity changes caused by disease-associated variants, to address the existence of additional multimer conformations, and to determine the effects of variants on de novo formation of TREM2 multimers.

A closer examination of the biological effects of multimerization will be key to designing future drugs targeting TREM2. Lacking this knowledge, small molecule drugs actively being designed to monovalently engage TREM2 may fail to replicate some multimerization-dependent effects seen in current antibody-based therapeutics. In addition, antibody-based therapeutics may have altered activity in patients with AD-associated variants due to changes in their ability to induce TREM2 multimerization. Altogether, a better understanding of TREM2 multimerization is key both to developing future drugs and to better understanding the mechanisms of TREM2 activation by drugs and in disease.

AUTHOR CONTRIBUTIONS

Hunter Dean: Conceptualization; investigation; formal analysis; writing–original draft. **Rory Greer**: Conceptualization; investigation; formal analysis; writing–original draft. **Shan-Zhong Yang**: Investigation; formal analysis. **Daniel Elston**: Investigation. **Thomas Brett**: Resources; writing–review and editing. **Erik Roberson**: Conceptualization; funding acquisition; supervision; writing–review and editing. **Yuhua Song**: Conceptualization; funding acquisition; supervision; writing–review and editing.

ACKNOWLEDGMENTS

CONFLICT OF INTEREST STATEMENT

E.D.R. serves on a data monitoring committee for Lilly, a scientific advisory board for AGTC, and an editorial board for the Society for Neuroscience; has received royalty income from Genentech; and is an inventor on patents and patent applications related to the neurodegenerative disease-associated protein tau. The authors declare that they have no other conflicts of interest with the contents of this article. Author disclosures are available in the supporting information.

DATA AVAILABILITY STATEMENT

The molecular dynamics trajectories and constructs used in this article are available to be shared at reasonable request to the corresponding authors. All other relevant data for this study are included in the article and its supplementary files.

CONSENT STATEMENT

No human subjects are in this study; consent was not necessary.

ORCID

Yuhua Song https://orcid.org/0000-0002-2583-850X

REFERENCES

1. Guerreiro RJ, Lohmann E, Brás JM, et al. Using exome sequencing to reveal mutations in TREM2 presenting as a frontotemporal dementia-like syndrome without bone involvement. *JAMA Neurol*. 2013;70(1):78-84.

2. Guerreiro R, Wojtas A, Bras J, et al. TREM2 variants in Alzheimer's disease. *N Engl J Med*. 2013;368(2):117-127.

3. Cuyvers E, Bettens K, Philtjens S, et al. Investigating the role of rare heterozygous TREM2 variants in Alzheimer's disease and frontotemporal dementia. *Neurobiol Aging*. 2014;35(3):726. e11-9.

4. Bellenguez C, Küçükali F, Jansen IE, et al. New insights into the genetic etiology of Alzheimer's disease and related dementias. *Nat Genet*. 2022;54(4):412-436.

5. Rayaprolu S, Mullen B, Baker M, et al. TREM2 in neurodegeneration: evidence for association of the p.R47H variant with frontotemporal dementia and Parkinson's disease. *Mol Neurodegener*. 2013;8:19.

6. Liu G, Liu Y, Jiang Q, et al. Convergent genetic and expression datasets highlight TREM2 in Parkinson's disease susceptibility. *Mol Neurobiol*. 2016;53(7):4931-4938.

7. Kleinberger G, Yamanishi Y, Suárez-Calvet M, et al. TREM2 mutations implicated in neurodegeneration impair cell surface transport and phagocytosis. *Sci Transl Med*. 2014;6(243):243ra86.

8. Kober DL, Alexander-Brett JM, Karch CM, et al. Neurodegenerative disease mutations in TREM2 reveal a functional surface and distinct loss-of-function mechanisms. *Elife*. 2016;5:e20391.

9. Sudom A, Talreja S, Danao J, et al. Molecular basis for the loss-of-function effects of the Alzheimer's disease-associated R47H variant of the immune receptor TREM2. *J Biol Chem*. 2018;293(32):12634-12646.

10. Dean HB, Roberson ED, Song Y. Neurodegenerative disease-associated variants in TREM2 destabilize the apical ligand-binding region of the immunoglobulin domain. *Front Neurol*. 2019;10(1252):1252.

11. Wang Y, Cella M, Mallinson K, et al. TREM2 lipid sensing sustains the microglial response in an Alzheimer's disease model. *Cell*. 2015;160(6):1061-1071.

12. Atagi Y, Liu C-C, Painter MM, et al. Apolipoprotein E is a ligand for triggering receptor expressed on myeloid cells 2 (TREM2). *J Biol Chem*. 2015;290(43):26043-26050.

13. Bailey CC, Devaux LB, Farzan M. The triggering receptor expressed on myeloid cells 2 binds apolipoprotein E. *J Biol Chem*. 2015;290(43):26033-26042.

14. Yeh FL, Wang Y, Tom I, Gonzalez LC, Sheng M. TREM2 binds to apolipoproteins, including APOE and CLU/APOJ, and thereby facilitates uptake of amyloid-beta by microglia. *Neuron*. 2016;91(2):328-340.

15. Schlepckow K, Monroe KM, Kleinberger G, et al. Enhancing protective microglial activities with a dual function TREM2 antibody to the stalk region. *EMBO Mol Med*. 2020;12(4):e11227.

16. Bouchon A, Hernández-Munain C, Cella M, Colonna M. A dap12-mediated pathway regulates expression of CC chemokine receptor 7 and maturation of human dendritic cells. *J Exp Med*. 2001;194(8):1111-1122.

17. Szykowska A, Chen Yu, Smith TB, et al. Selection and structural characterization of anti-TREM2 scFvs that reduce levels of shed ectodomain. *Structure*. 2021;29(11):1241-1252.e5.

18. Zhao P, Xu Y, Fan X, et al. Discovery and engineering of an anti-TREM2 antibody to promote amyloid plaque clearance by microglia in 5XFAD mice. *MAbs*. 2022;14(1):2107971.

19. Fassler M, Rappaport MS, Cuño CB, George J. Engagement of TREM2 by a novel monoclonal antibody induces activation of microglia and improves cognitive function in Alzheimer's disease models. *J Neuroinflammation*. 2021;18(1):19.

20. Cheng Q, Danao J, Talreja S, et al. TREM2-activating antibodies abrogate the negative pleiotropic effects of the Alzheimer's disease variant Trem2 R47H on murine myeloid cell function. *J Biol Chem*. 2018;293(32):12620-12633.

21. Webb B, Sali A. Comparative protein structure modeling using MODELLER. *Curr Protoc Bioinformatics*. 2016;54:5.6.1-5.6.37.

22. Case DA, Babin V, Berryman JT, et al. *AMBER14*. University of California, San Francisco; 2014.

23. The PyMOL Molecular Graphics System, Version 2.5 Schrödinger, LLC. https://pymol.org/support.html

24. Olsson MHM, Søndergaard CR, Rostkowski M, Jensen JH. PROPKA3: consistent treatment of internal and surface residues in empirical pKa predictions. *J Chem Theory Comput*. 2011;7(2):525-537.

25. Dolinsky TJ, Czodrowski P, Li H, et al. PDB2PQR: expanding and upgrading automated preparation of biomolecular structures for molecular simulations. *Nucleic Acids Res*. 2007;35:W522-W525.

26. Jurrus E, Engel D, Star K, et al. Improvements to the APBS biomolecular solvation software suite. *Protein Sci*. 2018;27(1):112-128.

27. Case DA, Ben-Shalom IY, et al. *AMBER18*. University of California, San Francisco; 2018.

28. The PyMOL Molecular Graphics System, Version 1.8 Schrodinger, LLC. https://pymol.org/support.html

29. Eisenberg D, Schwarz E, Komaromy M, Wall R. Analysis of membrane and surface protein sequences with the hydrophobic moment plot. *J Mol Biol*. 1984;179(1):125-142.

30. Maier JA, Martinez C, Kasavajhala K, Wickstrom L, Hauser KE, Simmerling C. ff14SB: improving the accuracy of protein side chain and backbone parameters from ff99SB. *J Chem Theory Comput*. 2015;11(8):3696-3713.

31. Phillips JC, Braun R, Wang W, et al. Scalable molecular dynamics with NAMD. *J Comput Chem*. 2005;26(16):1781-1802.

32. Yan Qi, Murphy-Ullrich JE, Song Y. Molecular and structural insight into the role of key residues of thrombospondin-1 and calreticulin in thrombospondin-1-calreticulin binding. *Biochemistry*. 2011;50(4):566-573.

33. Lu H, Isralewitz B, Krammer A, Vogel V, Schulten K. Unfolding of titin immunoglobulin domains by steered molecular dynamics simulation. *Biophys J*. 1998;75(2):662-671.

34. Wang C, Nguyen PH, Pham K, et al. Calculating protein-ligand binding affinities with MMPBSA: method and error analysis. *J Comput Chem*. 2016;37(27):2436-2446.

35. Miller BR, Mcgee TD, Swails JM, Homeyer N, Gohlke H, Roitberg AE. MMPBSA.py: an efficient program for end-state free energy calculations. *J Chem Theory Comput*. 2012;8(9):3314-3321.

36. Hall R, Dixon T, Dickson A. On calculating free energy differences using ensembles of transition paths. *Front Mol Biosci*. 2020;7:106.

37. Kabsch W, Sander C. Dictionary of protein secondary structure: pattern recognition of hydrogen-bonded and geometrical features. *Biopolymers*. 1983;22(12):2577-2637.

38. R Core Team. R: a language and environment for statistical computing. R Foundation for Statistical Computing, Vienna, Austria; 2023.

39. Decker Y, Németh E, Schomburg R, et al. Decreased pH in the aging brain and Alzheimer's disease. *Neurobiol Aging*. 2021;101:40-49.

40. Karczewski KJ, Francioli LC, Tiao G, et al. The mutational constraint spectrum quantified from variation in 141,456 humans. *Nature*. 2020;581(7809):434-443.

41. Carrasco K, Boufenzer A, Jolly L, et al. TREM-1 multimerization is essential for its activation on monocytes and neutrophils. *Cell Mol Immunol*. 2019;16(5):460-472.

42. Wang Y, Liu L, Davies DR, Segal DM. Dimerization of Toll-like receptor 3 (TLR3) is required for ligand binding. *J Biol Chem*. 2010;285(47):36836-36841.

43. Kucka K, Wajant H. Receptor oligomerization and its relevance for signaling by receptors of the tumor necrosis factor receptor superfamily. *Front Cell Dev Biol*. 2020;8:615141.

44. Van Driel IR, Davis CG, Goldstein JL, Brown MS. Self-association of the low density lipoprotein receptor mediated by the cytoplasmic domain. *J Biol Chem*. 1987;262(33):16127-16134.

45. Marques PE, Nyegaard S, Collins RF, et al. Multimerization and retention of the scavenger receptor SR-B1 in the plasma membrane. *Dev Cell*. 2019;50(3):283-295.e5.

46. Kober DL, Stuchell-Brereton MD, Kluender CE, et al. Functional insights from biophysical study of TREM2 interactions with apoE and Aβ_{1-42}. *Alzheimers Dement*. 2020;17(3):475-488.

47. Xue T, Ji J, Sun Y, et al. Sphingosine-1-phosphate, a novel TREM2 ligand, promotes microglial phagocytosis to protect against ischemic brain injury. *Acta Pharm Sin B*. 2022;12(4):1885-1898.

48. Shirotani K, Hori Y, Yoshizaki R, et al. Aminophospholipids are signal-transducing TREM2 ligands on apoptotic cells. *Sci Rep*. 2019;9(1):7508.

49. Song W, Hooli B, Mullin K, et al. Alzheimer's disease-associated TREM2 variants exhibit either decreased or increased ligand-dependent activation. *Alzheimers Dement*. 2017;13(4):381-387.

50. Boza-Serrano A, Ruiz R, Sanchez-Varo R, et al. Galectin-3, a novel endogenous TREM2 ligand, detrimentally regulates inflammatory response in Alzheimer's disease. *Acta Neuropathol*. 2019;138(2):251-273.

51. Hsieh CL, Koike M, Spusta SC, et al. A role for TREM2 ligands in the phagocytosis of apoptotic neuronal cells by microglia. *J Neurochem*. 2009;109(4):1144-1156.

52. Zhao Y, Wu X, Li X, et al. TREM2 is a receptor for beta-amyloid that mediates microglial function. *Neuron*. 2018;97(5):1023-1031.e7.

53. Lessard CB, Malnik SL, Zhou Y, et al. High-affinity interactions and signal transduction between Abeta oligomers and TREM2. *EMBO Mol Med*. 2018;10(11):e9027.

54. Pasquier B, Launay P, Kanamaru Y, et al. Identification of FcalphaRI as an inhibitory receptor that controls inflammation: dual role of FcRgamma ITAM. *Immunity*. 2005;22(1):31-42.

55. Barrow AD, Trowsdale J. You say ITAM and I say ITIM, let's call the whole thing off: the ambiguity of immunoreceptor signalling. *Eur J Immunol*. 2006;36(7):1646-1653.

56. Kober DL, Brett TJ. TREM2-ligand interactions in health and disease. *J Mol Biol*. 2017;429(11):1607-1629.

57. Wang S, Sudan R, Peng V, et al. TREM2 drives microglia response to amyloid-beta via SYK-dependent and -independent pathways. *Cell*. 2022;185(22):4153-4169.e19.

SUPPORTING INFORMATION

Additional supporting information can be found online in the Supporting Information section at the end of this article.